https://doi.org/10.1016/j.jallcom.2016.11.409

Photoluminescence, electro-optic response and piezoelectric properties in pressureless-sintered Er-doped KNN-based transparent ceramics

Xiao Wu, Shengbo Lu, K.W. Kwok*

Department of Applied Physics and Materials Research Centre

The Hong Kong Polytechnic University, Hung Hom, Kowloon, Hong Kong, China

ABSTRACT

Er-doped $(K_{0.5}Na_{0.5})_{1-x}Li_xNb_{1-x}Bi_xO_3$ ($0.05 \leq x \leq 0.08$) ceramics have been prepared by pressureless sintering. Because of the cubic-like phase as well as the dense and fine-grained structure, the ceramics are optically clear, exhibiting high transmittances in the near-infrared and mid-infrared (MIR) regions (~50% and ~75%, respectively). They also possess strong electro-optic (EO) response, giving a large effective linear EO coefficient (128-184 pm/V). Owing to Er^{3+}, the ceramics exhibit green and red up-conversion photoluminescence (PL) emissions, which are sensitive to the crystal symmetry of the ceramic host. The ceramics also exhibit a low absorption coefficient of OH^- groups and then distinct and broadband MIR emissions. Together with the relatively large piezoelectric coefficient (70-90 pC/N), high dielectric constant (~1400) and low dielectric loss (~0.03), the ceramics open up potential applications in electrical/optical interdisciplinary field, such as visible displays, MIR solid lasers and optical attenuators.

Keywords: transparent ceramics; photoluminescence; mid-infrared emission; electro-optic effect; ferroelectrics

* Corresponding author. Tel.: +852 27665667; fax: +852 23337629.

E-mail address: apkwkwok@polyu.edu.hk (K.W. Kwok)

1. Introduction

Materials possessing two or more functional properties have attracted considerable attention and become the interdisciplinary field of research [1,2]. Among various types of multifunctional materials, ferroelectric materials possessing characteristics of spontaneous polarization, domain structure and piezoelectric response have been extensively investigated for various applications [3,4]. It has been shown that after doping rare-earth ions (RE^{3+}), ferroelectric materials can exhibit both electrical (e.g. ferroelectric) and photoluminescence (PL) properties, and thus showing potential applications in multifunctional optoelectronic area [5].

Among RE^{3+}, Er^{3+} is a good activator because of its wide PL emission range, from visible (Vis) to mid-infrared (MIR) regions [6]. Owing to the promising achievement in laser output, Er-based solid-state lasers can be operated in the eye-safe MIR region, exhibiting applications in medical surgery, remote sensing, atmosphere pollution monitoring and military counter-measures [7]. Metal-oxide and metal-halide glasses, such as fluorides, tellurites, phosphates, germinates, bismuthates and their derivatives [8-12], are commonly investigated as the hosts of the Er-doped materials for obtaining intense MIR emission. The good glass hosts for MIR lasers are expected to contain low concentration of OH^- groups, which give an absorption band at ~3 μm and have significant effect on the MIR emission [10]. Although the glass hosts exhibit high optical transmittance in the MIR region, they have drawbacks such as fragility, manufacture difficulty and low laser-induced damage threshold [13], which limit their practical applications. Transparent ceramic oxide is a superior substitute for glasses

because of its better chemical durability, mechanical strength, thermal stability and good light transmission.

Ferroelectric materials, including both single crystals and transparent ceramics, possessing high optical transparency and strong electro-optic (EO) effect have been widely investigated [14,15]. Haertling and Land developed the first transparent EO ceramics $(Pb_{1-x}La_x)(Zr_yTi_{1-y})_{1-x/4}O_3$ (PLZT) in 1971. They are mainly relaxor ferroelectrics with a cubic-like perovskite structure [14]. However, because of high lead content, PLZT-based materials are harmful to the environment. Therefore, it is urgently needed to develop environmental-friendly lead-free EO ceramics. $K_{0.5}Na_{0.5}NbO_3$ (KNN) ceramic is considered as a promising candidate for lead-free ferroelectric ceramics because of its high Curie temperature (T_c ~420°C) and large electromechanical coupling coefficient (k_p ~45%) [16].

KNN-based transparent EO ceramics (i.e. $(K_{0.5}Na_{0.5})_{1-x}Li_xNb_{1-x}Bi_xO_3$, $0.05 \leq x \leq 0.09$) have been prepared using both the hot-press sintering and pressureless sintering techniques [17,18]. They exhibit a maximum optical transmittance of 70% in the MIR region and large effective linear EO coefficient in the range of 120-200 pm/V [17]. In this work, Er^{3+} ions will be doped in the KNN-based transparent ceramics for realizing multifunctionalities including PL characteristics as well as EO and ferroelectric responses. To the best of our knowledge, ceramic materials possessing both (practical) EO and PL properties have rarely been reported. And good piezoelectric performance is difficult to be achieved in transparent ceramics with a cubic symmetry. Recently, considerable work has been conducted on electric-field

tuning of PL, in particular the association between the PL response from the luminescent center and field-induced changes in the local symmetry of the host [19-21]. As a lead-free “luminescent ferroelectric”, Er-doped KNN-based transparent ceramics is a good candidate for studying the tuning PL response owing to its transparence for observation. Here Er-doped KNN-based transparent ceramics have been fabricated by pressureless sintering, and the crystal structures and microstructures have been studied. The relationship between phase structure evolution and change of up-conversion PL performance has been elaborated based on the Judd-Ofelt (J-O) theory. The transmittance, Vis and MIR emissions, EO response as well as electrical (especially good piezoelectric) properties have been investigated for multifunctional applications.

2. Experimental

$(K_{0.5}Na_{0.5})_{1-x}Li_xNb_{1-x}Bi_xO_3$ ceramics doped with 1 mol% Er (abbreviated as Er-KNNLB-x, x = 0, 0.05-0.08) were fabricated by pressureless sintering. The raw materials were analytical-grade K_2CO_3 (99.9%), Na_2CO_3 (99.5%), Nb_2O_5 (99.99%), Li_2CO_3 (99%), Bi_2O_3 (99.99%) and Er_2O_3 (99.99%). The powders in the stoichiometric ratio were first ball-milled thoroughly in anhydrous ethanol using zirconia balls for 12 h, then baked at 120°C and calcined at 850°C for 4 h. The calcined powers were ball-milled again for 12 h, dried and sieved through an 80-mesh screen. After that, they were mixed thoroughly with a polyvinyl alcohol binder solution and pressed into disk samples with the diameter of 12 mm and thickness of 1 mm under a pressure of 300 MPa. To completely burn out the binder and remove

pores, the samples were heated to 800°C at a slower rate of 0.5°C/min. After soaking at 800°C for 2 h, the disk samples were sintered at 1060-1100°C for 4 h in air for densification. All the sintered ceramics were polished by using 0.5 μm diamond paste to a thickness of 0.3 mm. Before the measurements of electrical properties, silver electrodes were fired on the top and bottom surfaces of the samples. Then the ceramics were poled under an electric field of 5 kV/mm at 150°C in silicone oil for 30 min.

The optical transmittances of the ceramics were measured in the range of 300-900 nm using a UV-Vis spectrophotometer (UV-2550, Shimadzu Co., Japan) and in the range of 1.5-10 μm by a Fourier Transform infrared (FTIR) spectrophotometer (Vertex 70, Bruker Co., Germany). The crystallite structures were examined using X-ray diffraction (XRD) analysis with CuK_α radiation (SmartLab, Rigaku Co., Japan). A general diffraction analysis program (MAUD) was used to refine the cell parameters based on the Rietveld method. The microstructures of the ceramics were observed using a scanning electron microscope (SEM) (JSM-6490, JEOL Ltd., Japan), while their domain structures were examined using a transmission electron microscope (TEM) (JEM-2100F, JEOL Ltd., Japan). The PL (both Vis and MIR) emission spectra were measured by a spectrophotometer (FLSP920, Edinburgh Instruments, UK) using a 980-nm diode laser as the excitation source. The EO properties were measured with a transverse geometry using a modified Sénarmont method, of which the details can be found elsewhere [22]. The wavelength of laser in the EO measurement is 633 nm. The dielectric constant (ε_r) and dielectric loss (tan δ)

were measured as functions of temperature using an impedance analyzer (HP 4194A, Agilent Technologies Inc., Palo Alto, CA). The ε_r and tan δ at room temperature were measured using an impedance analyzer (Agilent 4294A). A conventional Sawyer-Tower circuit was used to measure the polarization-electric field (*P*-*E*) hysteresis loops at 100 Hz. The piezoelectric coefficient (d_{33}) was measured using a piezo-d_{33} meter (ZJ-3A, China).

3. Results and discussion

The optical transmittances (T) spectra and a photograph of the Er-KNNLB-*x* ceramics are shown in Fig. 1. For the ceramics with $0.05 \leq x \leq 0.08$, the observed T increases steadily from zero as the wavelength increases from ~400 nm to ~900 nm, and then becomes saturated in the MIR range (2-5 μm). It can be seen that the ceramic with $x = 0.05$ exhibits the highest transmittance, giving an observed T of ~55% at ~900 nm and ~75% in the range of 2-5 μm. The Er-KNNLB-0 (i.e., Er-doped KNN) ceramic is opaque in the Vis range and the observed T in the MIR range is much lower than others. As illustrated in the inset of Fig. 1, the ceramics with $0.05 \leq x \leq 0.08$ are optically clear in spite of the difference in optical transmittances. Absorption bands (marked by dashed boxes), resulting from the transitions $^4I_{15/2} \rightarrow {}^2H_{11/2}/{}^4S_{3/2}$ (520-560 nm), $^4I_{15/2} \rightarrow {}^4F_{9/2}$ (640-680 nm) and $^4I_{15/2} \rightarrow {}^4I_{13/2}$ (1.45-1.55 μm) of Er^{3+}, respectively, are clearly observed in each spectrum. However, the absorption band arisen from OH^- groups at its wavelength (~3 μm) is hardly observed. This suggests that the ceramics contain a very low concentration of OH^- group, which can be practically characterized by an absorption coefficient α_{OH^-} [11]:

$$\alpha_{OH^-} = \ln(T_0 / T_1) / l \quad (1)$$

where T_0 is the transmittance at the base line, T_1 is the lowest transmittance at the wavelength of OH^- groups (i.e., ~3 μm), and l is the sample thickness. It has been known that, owing to the participation in the energy transfer process of RE^{3+}, the OH^- group can quench the PL emissions in the MIR region. Accordingly, a low concentration of OH^- groups (or a low α_{OH^-}) is desired for MIR laser materials [23]. The calculated α_{OH^-} values for the Er-KNNLB-*x* ceramics (with a thickness of 0.3 mm) are similar, in the range of 0.22-0.28 cm^{-1}, which are substantially lower than those of the glasses, such as phosphate glass (1.2 cm^{-1}) [24], tellurite-germanate glass (0.99 cm^{-1}) [25], bismuthate glass (0.575 cm^{-1}) [26], fluorotellurite glass (0.544 cm^{-1}) [25], and are comparable to those of ZrF_4-BaF_2-LaF_3-AlF_3-YF_3 (ZBLAY) glass (0.252 cm^{-1}) [24] and germanate glass (0.196 cm^{-1}) [11].

The XRD patterns of the Er-KNNLB-*x* ceramics are shown in Fig. 2a. All the ceramics possess a single-phase perovskite structure, suggesting that Li^+, Bi^{3+} and Er^{3+} ions have diffused into the corresponding sites of the KNN lattice. The diffraction peaks (220) and (002) of the ceramics merge together, indicating that the ceramics may transform into another phase. The lattice constants (a, b, c and β) of the ceramics have been refined using all the diffraction peaks by the Rietveld method. Both the orthorhombic and monoclinic models were used for the refinement and there was only small difference between them, which was probably due to the cubic-like crystal structure. And the monoclinic model provided better fit than the orthorhombic one, i.e. smaller reliability factor (R_{wp}) and goodness-of-fit indicator (S) values [17].

Thus, a monoclinic *Pm* model was used for the refinement. Table 1 lists the calculated lattice constants together with the R_{wp} and S. The low R_{wp} (< 15%) and S (< 2) values denote a good fit between the observed and calculated patterns. The fitted c/a value increases, while the difference between a and b decreases with increasing *x*. At *x* = 0.07, they reach a maximum value of 0.9988 and a minimum value of 0.0221 Å, respectively. This suggests that the crystal structure has transformed to a pseudo-cubic (or cubic-like) phase, and the Er-KNNLB-0.07 ceramic has a nearly cubic structure.

Fig. 2b shows, as an example, the SEM micrograph of the Er-KNNLB-0.06 ceramic. Similar results have also been observed for other Er-KNNLB-*x* ceramics. The ceramic has a dense and fine-grained (generally < 600 nm) structure with cuboid morphology. Probably due to the pressureless sintering, a small number of tiny pores are inevitably formed and distributed randomly in the ceramic. The translucency (in the Vis range) of the ceramics (Fig. 1) should be partly ascribed to the reduced optical scattering by the fine grains and small amount of pores. It has been shown that the light scattering at the grain-boundary becomes smaller if the grain size is smaller than the wavelength of light [27]. Nevertheless, the optical transparency of the pressureless-sintered ceramics is lower than that of the hot-press sintered ones [17]. Fig. 2c shows the bright field TEM image of a grain of the Er-KNNLB-0.06 ceramic and the selected area electron diffraction (SAED) pattern along the [110] zone axis. The domain walls are mostly along the {110} family planes. As viewed from the inter-angle of the domain walls, 60°/120° domain can be observed. Arrayed spots are clearly observed in the SAED pattern, indicating that the ceramic possesses high

crystallinity with a pseudo-cubic structure, consistent with the XRD results.

Fig. 3a shows the Vis up-conversion PL emission spectra of the Er-KNNLB-*x* ceramics. There are three emission bands: green emissions in 510-537 nm and 537-570 nm, and red emissions in 640-685 nm, which are attributed to the transitions $^{2}H_{11/2} \rightarrow {}^{4}I_{15/2}$, $^{4}S_{3/2} \rightarrow {}^{4}I_{15/2}$ and $^{4}F_{9/2} \rightarrow {}^{4}I_{15/2}$ of Er^{3+}, respectively. Probably due to different crystal structures, the emission spectra of the Er-KNNLB-*x* ceramics are of different shapes as compared with the other Er-doped KNN-based opaque ceramics, such as Er-KNN and Er-KNLN [6,28]. For an up-conversion luminescent material with a high Vis transparency, it is easy to achieve mutual superposition of both transmitting and emission light for laser gain. As a result, the effect of up-conversion abilities may be weakened and the pump power of NIR laser may slightly decrease [29]. It is then anticipated that the Er-KNNLB-*x* transparent ceramics can be used in laser applications.

As illustrated in Fig. 3d, Er^{3+} ions in the $^{4}I_{15/2}$ ground state are excited by the incident 980-nm photons to the $^{4}I_{11/2}$ level by a ground state absorption (GSA) process. Some of the Er^{3+} ions in $^{4}I_{11/2}$ level absorb one more incident photon to populate the $^{4}F_{7/2}$ level by an excited state absorption (ESA) process. Multi-phonon relaxation (MPR) processes then take place, populating the $^{2}H_{11/2}$, $^{4}S_{3/2}$, and $^{4}F_{9/2}$ levels by nonradiative relaxation. Ultimately, Er^{3+} ions relax radiatively to the ground state $^{4}I_{15/2}$, producing the green ($^{2}H_{11/2}/^{4}S_{3/2} \rightarrow {}^{4}I_{15/2}$) and red ($^{4}F_{9/2} \rightarrow {}^{4}I_{15/2}$) emissions. The variations of the relative integrated PL intensity of the green and red emission bands are shown in Fig. 3b. The Er-KNNLB-0.08 ceramic exhibits the highest PL intensity

while the Er-KNNLB-0.07 ceramic exhibit the lowest, showing a decrease of ~18% and ~14% in the PL intensities of the green and red emissions, respectively. The ratio of the PL intensities of the red and green emissions (I_r/I_g) for the Er-KNNLB-0.07 ceramic is largest. These should be attributed to the structural transformation arisen from the doping of Li^+ and Bi^{3+}.

It has been known that the PL performance is affected by the crystal field and symmetry of the host [30]. According to the J-O theory [31,32], the spontaneous transition probability A_{ed} for the Vis 4*f*-4*f* emissions of Er^{3+} (which are mainly electric dipole transitions) can be expressed as [33]:

$$A_{ed} = \frac{64\pi^4 e^2}{3h(2J+1)\lambda^3}\left[\frac{n(n^2+2)^2}{9}\right]S_{ed} \quad (2)$$

where e is the charge of a proton, h is the Planck constant, J is the total angular momentum quantum number of the initial level, λ is the mean wavelength of the transition, n is the refractive index and S_{ed} is the electric dipole line strength which is given as:

$$S_{ed} = \sum_{t=2,4,6} \Omega_t \left| \left\langle 4f(S,L)J \left\| U^{(t)} \right\| 4f(S',L')J' \right\rangle \right|^2 \quad (3)$$

where $|4f(S,L)J\rangle$ and $|4f(S',L')J'\rangle$ are the initial and final states, respectively, in the electric dipole transition, $\langle\|U^{(t)}\|\rangle$ are the double reduce matrix elements of unit tensor operators which are considered to be independent of the host material, and Ω_t are the phenomenological J-O parameters which depend on the crystal field and radial integrals of an electron [34]. It has been shown that the transition probability of the hypersensitive green emissions of Er^{3+} is dependent on Ω_2, which has a close

relationship with the symmetry of Er^{3+} sites in the host. A high crystal symmetry leads to a low Ω_2 and then a weak green emission. Accordingly, the lowest PL intensity of the green emission observed for the Er-KNNLB-0.07 ceramic should be partly attributed to its nearly cubic structure as revealed by the XRD results (Fig. 2a and Table 1). On the other hand, the red emission is less sensitive to the crystal symmetry and depends on the other two parameters Ω_4 and Ω_6 (which are related to the covalency of the host) [26,35]. The variations in the PL intensity of the red emission may then be merely due to the changes in the sizes of the domains and grains, which affect the light scattering at their boundaries. Indeed, the green emissions will also be affected in a similar manner. Moreover, as most of the electrons dwelled in the $^4F_{9/2}$ level are populated from the upper $^4S_{3/2}$ level by MPR processes, the tendency for the red emission may then follow that of the green emissions (Fig. 3b). Recently, it has been shown that, due to the different dependences on crystal symmetry, the PL intensity ratio I_r/I_g for Er-doped $Pb(Mg_{1/3}Nb_{2/3})O_3$-$PbTiO_3$ ceramics can effectively reveal the change in the phase structure of the ceramic host, i.e., a decrease in crystal symmetry is clearly indicated by a drop in I_r/I_g [33]. Therefore, the observed maximum I_r/I_g ratio for the Er-KNNLB-0.07 ceramic (Fig. 3b) reconfirms that it possesses the highest symmetry (nearly cubic structure) among the samples.

Fig. 3c shows the MIR emissions of the Er-KNNLB-*x* ceramics. The broad emission bands centered at ~2.75 μm are attributed to the transition $^4I_{11/2} \rightarrow {}^4I_{13/2}$ of Er^{3+} (Fig. 3d). Probably due to the less sensitivity to the crystal symmetry [35], the observed PL intensity only varies slightly for different samples. The full width at half

maximum (FWHM) value of the MIR emissions are ~180 nm, which is larger than most of the glass hosts, such as Er-doped germanate glasses (~100 nm) [11], Er-doped oxysulfide glasses (~130 nm) [36] and Er-doped fluorotellurite glasses (~163 nm) [37]. A broad emission band is beneficial to widening the wavelength range of MIR laser sources. As the stretching vibration of free OH^- groups and the absorption arisen from hydrogen bonds occurs at ~3 μm [38], the OH^- groups will participate in the energy transfer processes of Er^{3+} and then reduce the MIR emission intensity [11]. Hence, the distinct MIR emissions of the ceramics are mainly due to the low content of OH^- groups (the small values of α_{OH^-}). Combined with the high transmittance in the MIR range (Fig. 1) and distinct MIR emissions, the Er-KNNLB-*x* transparent ceramics should have potential applications in high-power ~2.7-μm (MIR) solid lasers.

EO response of the Er-KNNLB-*x* ceramics has been investigated. The field-induced birefringence δ(Δn) as a function of electric field E for the ceramics is shown in Fig. 4. It can be seen that all the ceramics exhibit a good linear relationship between δ(Δn) and E. The general expression for the linear EO effect (Pockels effect) is given as [17]:

$$\delta(\Delta n) = \frac{1}{2} n_e^3 \gamma_c E \tag{4}$$

where n_e is the refractive index for light with the vibrating electric-field parallel to the optical axis (i.e., the polarization axis of the sample), γ_c is the effective linear EO coefficient. The n_e value of the ceramics is ~2.26 at 633 nm (experimental value of the KNNLB ceramic) [17], which is lower than that of PLZT transparent ceramics (~2.5)

[39] and very close to $LiNbO_3$ single crystals (2.2-2.28) [40]. By using the (fitted) slop of the curves, γ_c for the ceramics are estimated and listed in Table 2. The observed γ_c for the Er-KNNLB-*x* (*x* = 0.05-0.08) ceramics are quite large, in the range of 128-184 pm/V, which are close to that of the hot-press-sintered KNNLB ceramics [17], indicating that the pressureless-sintering method and Er-doping do not deteriorate the EO performance. Large γ_c should be partly due to the large ε_r values of the ceramics (Table 2) [41]. Although the observed γ_c are not as large as that of $Pb_{0.92}La_{0.08}(Zr_{0.65}Ti_{0.35})_{0.98}O_3$ transparent ceramics (612 pm/V), they are about 6-9 times larger than that of lead-free $LiNbO_3$ single crystals (19.9 pm/V) [42] and comparable to that of $0.67Pb(Mg_{1/3}Nb_{2/3})O_3$-$0.33PbTiO_3$ single crystals (182 pm/V) [22]. The Er-KNNLB-*x* transparent ceramics can be applied in variable optical attenuator (VOA) which requires small-sized and environmentally friendly EO materials with large EO coefficient and high transmittance. The up-conversion PL properties allow the use of near-infrared (e.g., 980 nm) laser instead of Vis laser for testing or maintenance. As a result, the photodamage can be reduced and the service life of the VOA devices can be effectively extended.

Fig. 5a shows, as an example, the temperature dependences of ε_r and tan δ measured at different frequencies for the Er-KNNLB-0.06 ceramic. Similar results have been observed for other Er-KNNLB-*x* ceramics. The ceramic exhibits a broadened tetragonal-cubic transition peak, suggesting that a diffuse phase transition is induced. This should be due to the disordered structure and local compositional fluctuation resulting from the B-site replacement, i.e. Bi^{3+} can enter the B-site to

replace Nb^{5+}. As Li^+ (0.68 Å) has a smaller radius than K^+ and Na^+ (1.38 and 0.97 Å, respectively), the doping of Li^+ should be favorable for forming an ordered structure and then would not enhance the diffuseness of the phase transition [28]. It can also be seen that the observed ε_r decreases as the frequency increases from 1 kHz to 1 MHz. However, unlike a typical relaxor ferroelectric, the observed T_m (the temperature of maximum ε_r) does not increase with increasing frequency. Although it has been shown that the change in T_m for KNN-based relaxors is not very large, only about 7°C as the frequency increases [43], the Er-KNNLB-*x* ceramics may not be a typical relaxor and possess only relaxor-like characteristics [44]. Nevertheless, the ceramic exhibits a low dielectric loss (< 4.5%) in the temperature range of 25-350°C (Fig. 5a), suggesting that it should have a good potential for high temperature applications.

Probably due to the relaxor-like characteristics as well as the fine grains and cubic-like symmetry, the *P*-*E* loops of the Er-KNNLB-*x* ceramics become slant and flatted, as shown in Fig. 5b. For comparison, the *P*-*E* loop as well as the electrical properties of an Er-KNN (i.e., Er-KNNLB-0) opaque ceramic has also been measured, giving the results shown in Fig. 5b and Table 2, respectively. As shown in Table 2, the observed electric coercive fields (E_c) of the Er-KNNLB-*x* ceramics become larger while the observed remnant polarizations (P_r) are smaller as compared to the Er-KNN ceramic. Nevertheless, their dielectric properties of the Er-KNNLB-*x* ceramics improved, i.e., the observed ε_r becomes larger and tan δ becomes smaller than those of the Er-KNN ceramic. Meanwhile, they possess relatively good piezoelectric properties with the piezoelectric coefficients (d_{33}) of 70-90 pC/N. The good PL, EO

and piezoelectric performances enable the Er-KNNLB-*x* transparent ceramics to have multiple functions.

4. Conclusions

Er-KNNLB-*x* transparent ceramics have been fabricated by pressureless sintering. The ceramics possess a dense and fine-grain structure. The observed transmittance reaches a high value of ~55% at ~900 nm and ~75% in the MIR region. The good optical transparency should be due to the cubic-like crystal structure and relaxor-like characteristics, which have been attested by the XRD patterns, the temperature dependences of ε_r and *P-E* loops. Our results show that the green up-conversion emission of Er^{3+} is sensitive to the crystal symmetry of the KNNLB-*x* ceramic host, and the ratio of red to green emission intensities (I_r/I_g) is an effective parameter for indicating the symmetry change. Besides the Vis emissions, the ceramics have low absorption coefficients of OH^- groups and then distinct MIR emissions, showing potential applications in MIR solid-lasers. The ceramics also exhibit a large effective linear EO coefficient (128-184 pm/V), which make them suitable for VOA devices. Owing to the simultaneously outstanding EO effect, distinct Vis and broadband MIR PL emissions, large piezoelectric coefficients (70-90 pC/N), as well as good ferroelectric and dielectric properties, the Er-KNNLB-*x* transparent ceramics should have great application potentials in multifunctional optoelectronic areas.

Acknowledgements

This work was supported by the Research Grants Council of the Hong Kong

Special Administrative Region (Project No. PolyU 5170/13E and PolyU 5176/12E) and the Centre for Smart Materials of The Hong Kong Polytechnic University.

References

[1] D.F. Peng, X.S. Wang, C.N. Xu, X. Yao, J. Lin, T.T. Sun, J. Am. Ceram. Soc. 96 (2013) 184–190.

[2] L.T. Canham, Appl. Phys. Lett. 57 (1990) 1046–1048.

[3] H. Lu, C.W. Bark, D.E. Ojos, J. Alcala, C.B. Eom, G. Catalan, A. Gruverman, Science 336 (2012) 59–61.

[4] Q.Y. Yue, L.H. Luo, X.J. Jiang, W.P. Li, J. Zhou, J. Alloy. Compd. 610 (2014) 276–280.

[5] Y.B. Wei, Z. Wu, Y.M. Jia, J. Wu, Y.C. Shen, H.S. Luo, Appl. Phys. Lett. 105 (2014) 042902.

[6] X. Wu, C.M. Lau, K.W. Kwok, J. Lumin. 155 (2014) 343–350.

[7] L.Y. Zhang, Z.H. Yang, Y. Tian, J.J. Zhang, L.L. Hu, J. Appl. Phys. 110 (2011) 093106.

[8] Y. Tian, R.R., Xu, L.L. Hu, J.J. Zhang, J. Am. Ceram. Soc. 94 (2011) 2289–2291.

[9] H. Zhong, B. Chen, G. Ren, L. Cheng, L. Yao, J. Sun, J. Appl. Phys. 106 (2009) 083114.

[10] Y. Tian, R.R. Xu, L.Y. Zhang, L.L. Hu, J.J. Zhang, Opt. Lett. 36 (2011) 109–111.

[11] R.R. Xu, Y. Tian, L.L. Hu, J.J. Zhang, Opt. Lett. 36 (2011) 1173–1175.

[12] Y.Y. Guo, Y. Tian, L.Y. Zhang, L.L. Hu, N.K. Chen, J.J. Zhang, Opt. Lett. 37

(2012) 3387–3389.

[13] X.R. Hou, S.M. Zhou, W.J. Li, Y.K. Li, H. Lin, H. Teng, T.T. Jia, J. Am. Ceram. Soc. 93 (2010) 2779–2782.

[14] G.H. Haertling, C.E. Land, J. Am. Ceram. Soc. 54 (1971) 1–11.

[15] Y. Lin, B. Ren, X. Zhao, D. Zhou, J. Chen, X. Li, H. Xu, D. Lin, H. Luo, J. Alloy. Compd. 507 (2010) 425–428.

[16] X. Wu, K.W. Kwok, F.L. Li, J. Alloy. Compd. 580 (2013) 88–92.

[17] F.L. Li, K.W. Kwok, J. Eur. Ceram. Soc. 33 (2013) 123–130.

[18] F.L. Li, K.W. Kwok, J. Am. Ceram. Soc. 96 (2013) 3557–3562.

[19] J.H. Hao, Y. Zhang, X.H. Wei, Angew. Chem. Int. Ed. 50 (2011) 6876−6880.

[20] D.K. Khatua, A. Kalaskar, R. Ranjan, Phys. Rev. Lett. 116 (2016) 117601.

[21] H.L. Sun, X. Wu, T.H. Chung, K.W. Kwok, Sci. Rep. 6 (2016) 28677.

[22] X. Wan, D.Y. Wang, X. Zhao, H. Luo, H.L.W. Chan, C.L. Choy, Solid State Commun. 134 (2005) 547−551.

[23] M. Pollnau, E. Heumann, G. Huber, Appl. Phys. A 54 (1992) 404–410.

[24] Y. Tian, R.R. Xu, L.L. Hu, J.J. Zhang, J. Quant. Spectrosc. Radiat. Transfer. 113 (2012) 87–95.

[25] Y.Y. Guo, M. Li, L.L. Hu, J.J. Zhang, J. Phys. Chem. A 116 (2012) 5571−5576.

[26] Y. Y. Guo, M. Li, L.L. Hu, and J. J. Zhang, Opt. Lett. 37 (2012) 268−270.

[27] R. Apetz, M.P.B.V. Bruggen, J. Am. Ceram. Soc. 86 (2003) 480−486.

[28] X. Wu, K.W. Kwok, J. Am. Ceram. Soc. 97 (2014) 1504−1510.

[29] M. Suárez, A. Fernández, J.L. Menéndez, M. Nygren, Z. Zhao, R. Torrecillas, A.

Pablo, P. Haro-González, J.J. Romero, I.R. Martín, Ceram. Int. 40 (2014) 15951–15956.

[30] S.Y. Kang, Y.H. Kim, J. Moon, K.S. Kang, J. Appl. Phys. 48 (2009) 052301.

[31] B.R. Judd, Phys. Rev. 127 (1962) 750−761.

[32] G. S. Ofelt, J. Chem. Phys. 37 (1962) 511−520.

[33] Y.J. Yao, L.H. Luo, W.P. Li, J. Zhou, F.F. Wang, Appl. Phys. Lett. 106 (2015) 082906.

[34] S. Tanabe, T. Ohyagi, N. Soga, T. Hanada, Phys. Rev. B 46 (1992) 3305−3310.

[35] M.J. Weber, Phys. Rev. 157 (1967) 262−272.

[36] L.D. Vila, N. Aranha, Y. Messaddeq, E.B. Stucchi, S.J.L. Ribeiro, L.A.O. Nunes, J. Alloy. Compd. 344 (2002) 226–230.

[37] H. Zhan, Z.G. Zhou, J.L. He, A.X. Lin, Opt. Lett. 37 (2012) 3408–3410.

[38] G.N. Wang, S.X. Dai, J.J. Zhang, S.Q. Xu, L.L. Hu, Z.H. Jiang, Non-Cryst. Solids 351 (2005) 2147−2151.

[39] P.D. Thacher, Ferroelectrics 3 (1972) 147−150.

[40] D.E. Zelmon, D.L. Small, D. Jundt, J. Opt. Soc. Am. B 14 (1997) 3319−3322.

[41] M. DrDomenico, S.H. Wemple, J. Appl. Phys. 40 (1969) 720−734.

[42] M. Aillerie, M. D. Fontana, F. Abdi, C. Carabatos-Nedelec, N. Theofanous, G. Alexakis, J. Appl. Phys. 65 (1989) 2406−2408.

[43] Y. Guo, K. Kakimoto, H. Ohsato, J. Phys. Chem. Sol. 65 (2004) 1831−1835.

[44] H.L. Du, W.C. Zhou, F. Luo, D.M. Zhu, S.B. Qu, Z.B. Pei, J. Appl. Phys. 105 (2009) 124104.

Table 1 Lattice constants of the Er-KNNLB-x ceramics.

x	a (Å)	b (Å)	c (Å)	β (°)	a-b (Å)	c/a	R_{wp} (%)	S
0.05	3.9964	3.9613	3.9783	89.66	0.0351	0.9955	11.79	1.33
0.06	3.9959	3.9659	3.9875	89.83	0.03	0.9979	12.97	1.49
0.07	3.9934	3.9713	3.9886	89.84	0.0221	0.9988	12.73	1.46
0.08	3.9965	3.9723	3.9833	89.92	0.0242	0.9967	12.82	1.46

Table 2 The piezoelectric, dielectric, ferroelectric properties and effective EO coefficients of the Er-KNNLB-*x* ceramics.

x	γ_c (pm/V)	d_{33} (pC/N)	ε_r @1kHz	tan δ @1kHz	P_r (μC/cm^2)	E_c (kV/mm)
0	/	92	480	0.049	12.1	1.05
0.05	128	73	1347	0.033	7.1	1.18
0.06	184	89	1396	0.030	6.4	1.22
0.07	170	84	1332	0.035	5.8	1.21
0.08	182	80	1311	0.038	6.2	1.16

Figure Captions

Fig. 1 The optical transmittances and photograph of the Er-KNNLB-*x* ceramics.

Fig. 2 (a) XRD patterns of the Er-KNNLB-*x* ceramics, (b) SEM micrograph of the Er-KNNLB-0.06 ceramic, (c) Bright field TEM images of a grain and SAED pattern along [011] zone axis of the Er-KNNLB-0.06 ceramic.

Fig. 3 (a) Vis up-conversion PL emissions of the Er-KNNLB-*x* ceramics, (b) the variations of green and red emission intensities and ratio of red to green emission intensities (I_r/I_g) with *x*, (c) MIR emission spectra of the ceramics and (d) energy levels diagram of Er^{3+} ions.

Fig. 4 The variations of the field-induced birefringence with the amplitude of an ac voltage at 1 kHz for the Er-KNNLB-*x* ceramics.

Fig. 5 (a) Temperature dependences of ε_r and tan δ measured at frequencies in the range of 1 kHz to 1 MHz for the Er-KNNLB-0.06 ceramic, (b) *P-E* loops of the Er-KNNLB-*x* ceramics at 100 Hz.

Highlights

- Transparent ceramics Er-KNNLB-*x* have been fabricated by pressureless sintering.
- The ceramics show good photoluminescence and electro-optic properties.
- The ratio of red to green emission intensities is sensitive to the host symmetry.
- The ceramics possess high MIR transmittance and broadband MIR emissions.
- The ceramics may be applied in displays, MIR solid lasers and optical attenuators.

Fig. 1

Click here to download high resolution image

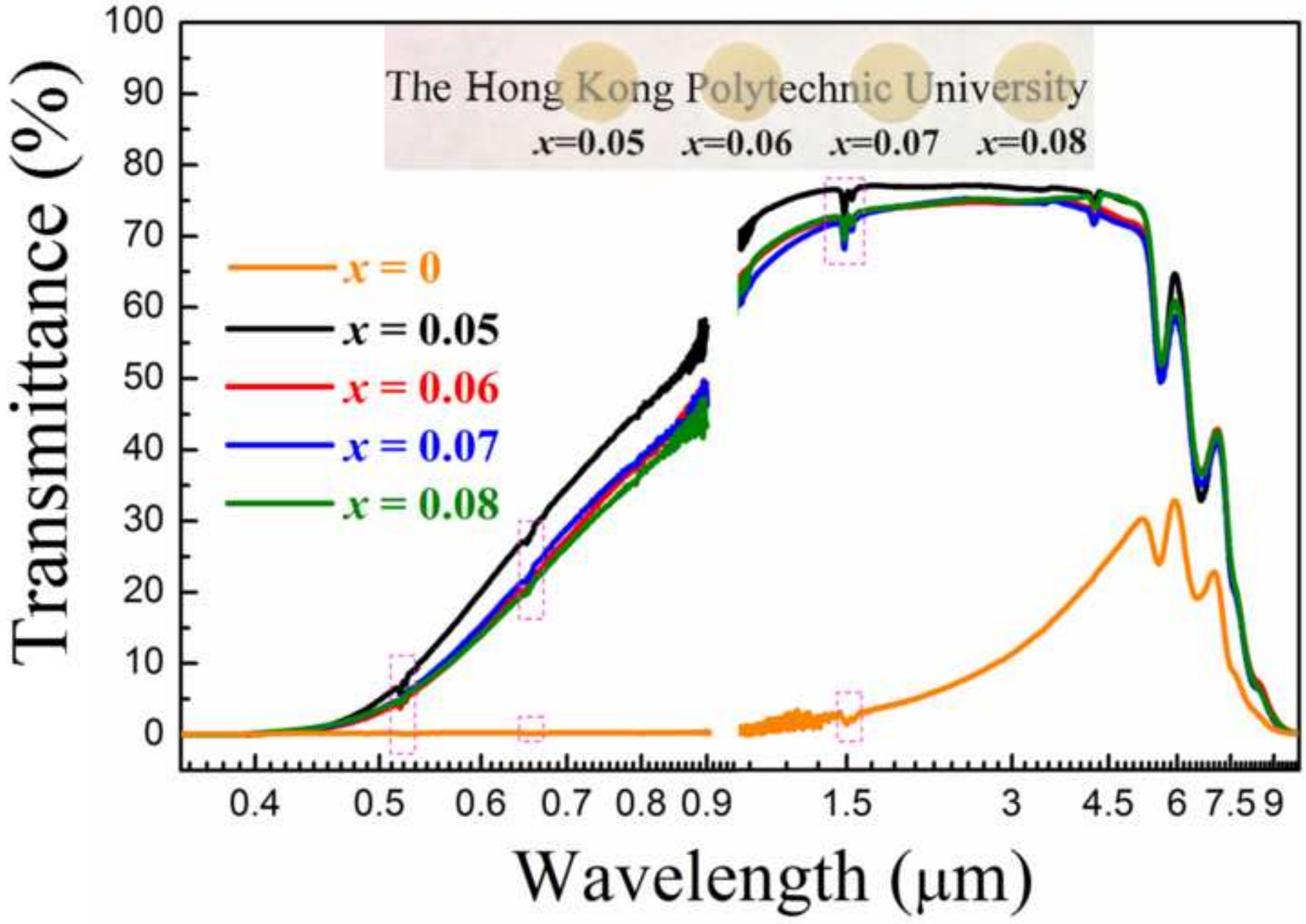

Fig. 2

Click here to download high resolution image

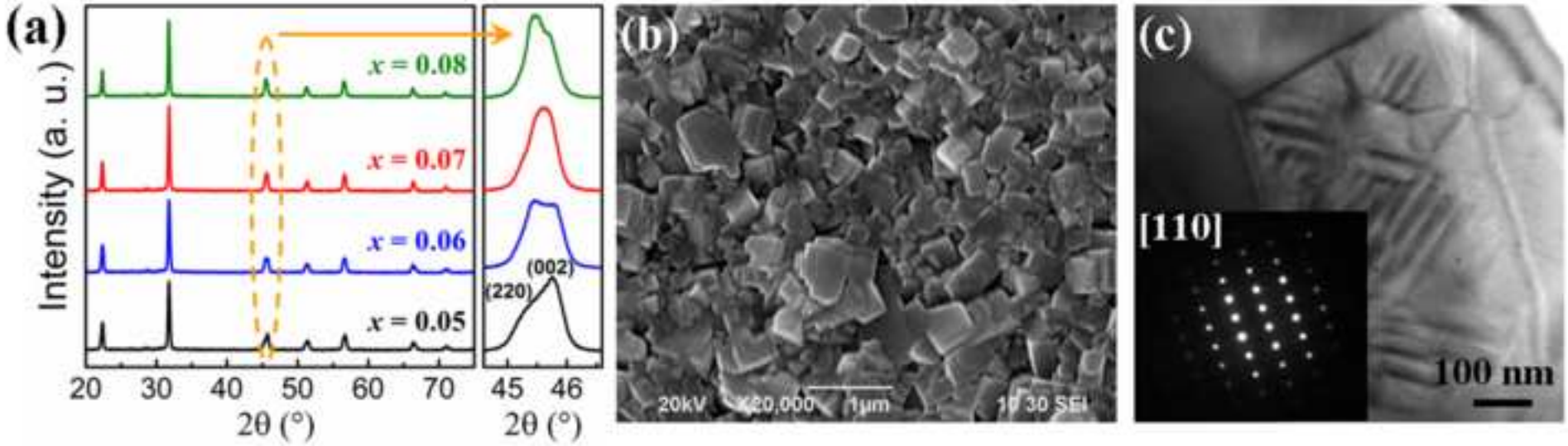

Fig. 3

Click here to download high resolution image

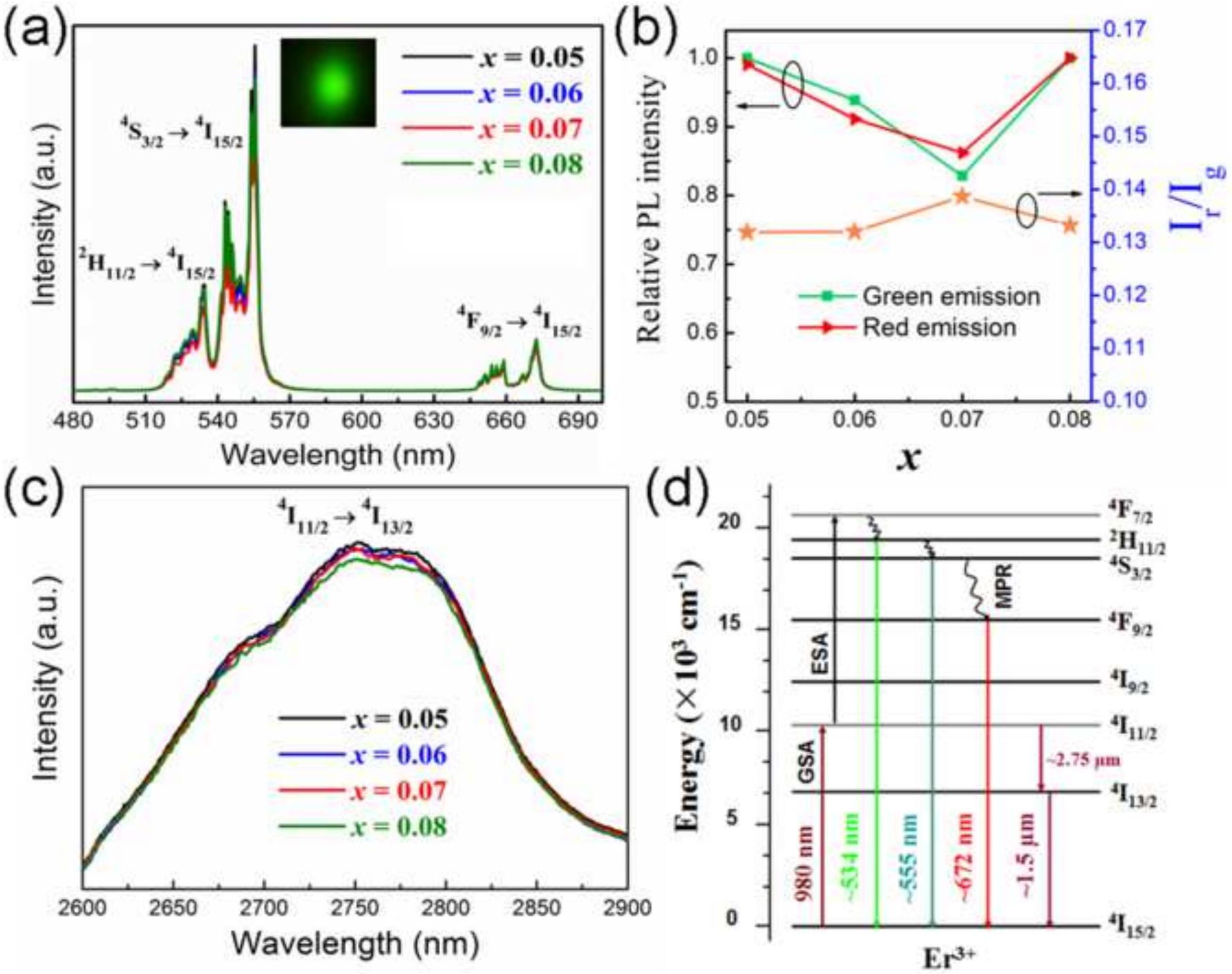

Fig. 4

Click here to download high resolution image

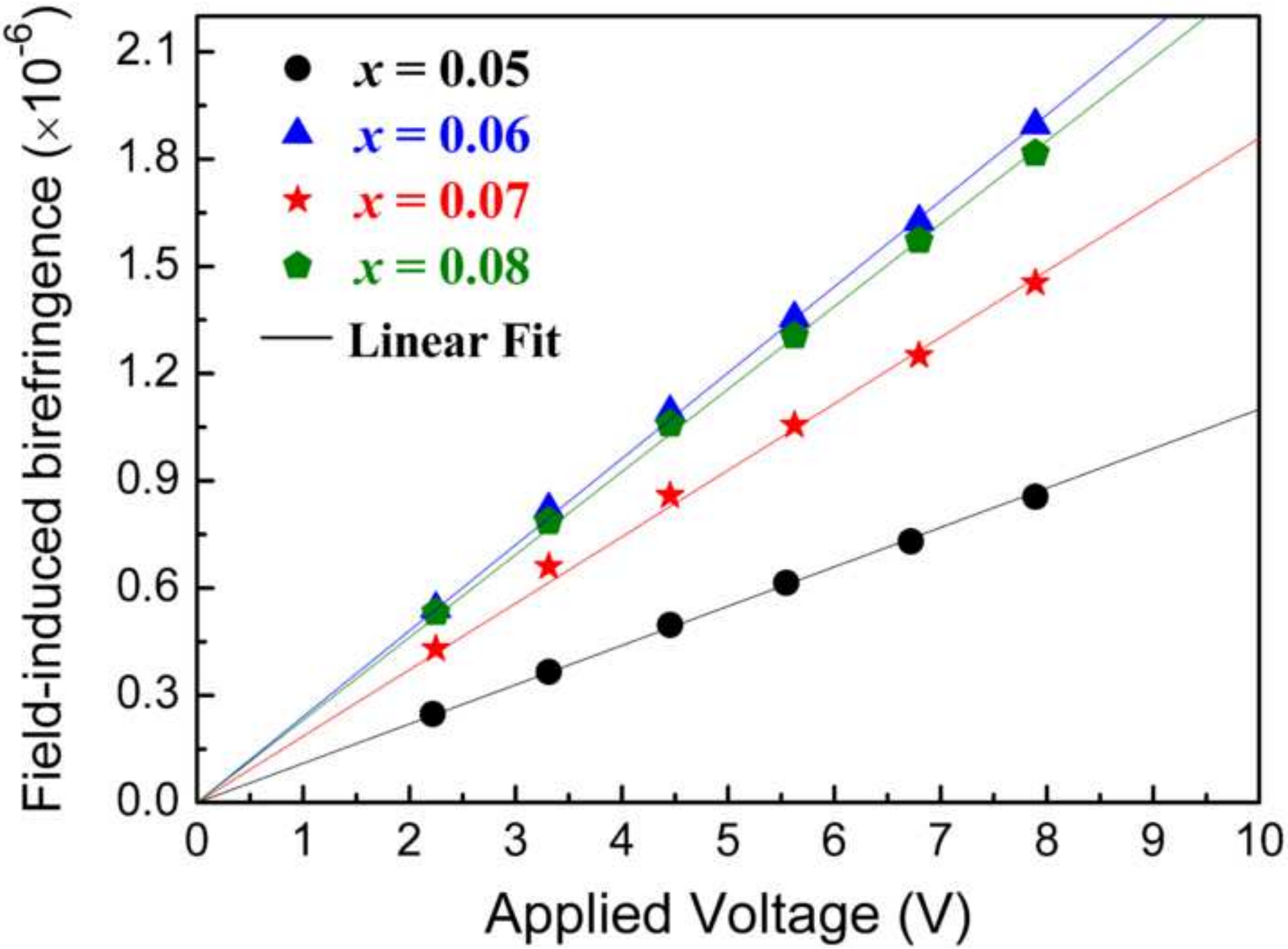

Fig. 5

Click here to download high resolution image